Mathematical and Computational Applications

MDPI

Article

Radiative Transport in Concentrated Viscoelastic Flow of HNF ($Cu–Fe_3O_4/C_2H_6O_2$) with the Cattaneo–Christov Model: Applications to Advanced Energy and Thermal Management Technologies

Rajab Alsayegh

Department of Mechanical Engineering, Faculty of Engineering, King Abdulaziz University, P.O. Box 80200, Jeddah 21589, Saudi Arabia; ralsayegh@kau.edu.sa

Abstract

Hybrid nanofluids with enhanced thermal conductivity have emerged as promising candidates for efficient heat removal in advanced energy systems and next-generation thermal management technologies. In particular, the use of viscoelastic base fluids embedded with radiatively active nanoparticles enables improved thermal regulation in solar collectors, electronic cooling units, and high-temperature industrial processes. This study presents a comparative thermal investigation of mono- and hybrid nanofluids comprising the ferro-oxide (Fe_3O_4) and copper (Cu) metallic particles dispersed in ethylene glycol ($C_2H_6O_2$), under magnetohydrodynamic (MHD) viscoelastic flow over a stretched surface. Accurate modeling of heat and mass phenomena in such fluids arises from their growing application in advanced thermal systems, including cooling technologies, electronic devices, and renewable energy modules. Unlike conventional models, the current analysis incorporates the Cattaneo–Christov heat flux framework to capture non-Fourier thermal relaxation effects, alongside the influence of thermal radiation and solutal transport. The developed system is truncated into dimensionless form with the proper choice of appropriate quantities, whose solution methodology is based on the implementation of a Runge–Kutta scheme. Compiled observations suggest that the hybrid nanomaterial exhibits more pronounced thermal recovery, while mono nanofluid attributes lower impact. Moreover, increasing the viscoelastic and magnetic parameters leads to notable variations in temperature and concentration distributions. This work advances the current literature by simultaneously integrating viscoelastic rheology, dual nanoparticle suspensions, and non-classical heat conduction laws, providing new insights for optimizing thermal performance in engineering applications.

Keywords: hybrid nanofluid; Cattaneo–Christov model; thermal radiation; shooting method; ethylene glycol-based suspension

Check for updates

Academic Editor: Gianluigi Rozza

Received: 20 April 2026
Revised: 6 July 2026
Accepted: 7 July 2026
Published: 9 July 2026

Copyright: © 2026 by the author. Licensee MDPI, Basel, Switzerland. This article is an open access article distributed under the terms and conditions of the Creative Commons Attribution (CC BY) license.

1. Introduction

1.1. Literature Survey

Many engineers now consider nanofluids the next wave of cooling liquids. They are created by dispersing extremely small solid particles (only a few nanometers wide) into everyday base fluids like ethylene glycol, oil-based materials, linear alpha olefins, and water. Such materials can be imposed in metals, carbon-based materials or metal oxides to improve the fluid's ability to conduct heat. Due to this enhancement, nanofluids have

novel relevance in industrial systems cooling, HVAC units and heat exchangers. In renewable energy, adding nanoparticles to the coolant boosts the performance of solar thermal collectors and geothermal plants. Researchers are even looking at medical uses: some nanofluids can carry drugs and deliver them to specific cells or tumors. Special applications of nanofluids are observed in nuclear reactor cooling and automotive radiators, where a nanoparticle-infused coolant can achieve the same heat dissipation with smaller, lighter hardware. Essentially, the suspended nanoparticles lead to a speeding up of both conduction and convection. Scientists continue studying these complex fluids under different flow and heating conditions, aiming to optimize their heat-transfer performance in each application. Hassan et al. [1] examined the convective nanofluid transport through a porous medium over a wavy surface, with a focus on the undulations' effects. Nadeem et al. [2] predicted the behavior of a Maxwell liquid with magnetic relevance on a vertically moving surface. They mentioned that the addition of nanomaterials to the non-Newtonian flow leads to the improvement of heat transfer. Oudina and Chabani [3] presented a review of nanofluid formulations and enclosure shapes to summarize how these approaches enhance thermal performance. Moreover, Bhatti et al. [4] performed simulations to improve thermal transport in confined geometries by incorporating third-grade hybrid nanofluids (HNFs) and electro-magneto-hydrodynamic effects, with the goal of optimizing energy systems. Siddiqui and Turkyilmazoglu [5] successfully modeled results for the film flow behavior of nano-micropolar fluids under viscous dissipation, offering insights into microscale fluid film dynamics for heat control. The role of nanoparticle aggregation, slip conditions, and viscosity variation in a rotating nanofluid environment, reflecting the complex interaction of unsteady thermal effects, was reported by Khan et al. [6]. Gupta and Wakif [7] implemented a neural network-based approach to explore heat and mass transfer between rotating disks using nanofluids. Puneeth et al. [8] incorporated gyrotactic microorganisms and slip boundary conditions; this investigation assessed bio-convective nanofluid flow around a stretching cylinder under Thompson–Troian slip effects. Using a different approach, Galal et al. [9] investigated channel flow for nanofluid by accomplishing a novel KKL model. Results governed by wedge flow of nanofluid with chemical species were focused on by the proposed model of Hamid et al. [10]. The behavior of silver-based nanoliquid near a Riga surface, comparing three binary nanofluid combinations for variations in thermophysical responses, was visualized by Gangadhar et al. [11]. Reddy et al. [12] used the homotopy analysis method to study two-phase flow of nanofluid by including entropy optimization applications.

Hybrid nanofluids (HNFs) are an advanced type of nanofluid created by dispersing two or more different kinds of nanoparticles. In an HNF, each type of nanoparticle contributes its own thermal advantages. Thus, HNFs transfer heat more effectively while being more stable. This makes HNFs attractive for many energy-intensive applications. For instance, HNFs have shown better performance in solar thermal systems by transferring heat more efficiently. HNFs are also used in other areas such as nuclear reactor cooling, chemical processing, and industrial cooling operations. In the electronics field, these hybrid fluids help maintain thermal stability by efficiently dissipating heat from high-performance microprocessors and integrated circuits. Owing to their multifunctional behavior and adaptability, hybrid nanofluids are at the forefront of thermal engineering research aimed at optimizing energy systems and next-generation cooling technologies. Results analyzed for non-Fourier modeling of nanofluid were referred to the study of Ramesh et al. [13]. Similarly, Manzoor et al. [14] presented an investigation of the enhancement of heat transfer in an HNF MHD flow over a moving sheet. Nasir et al. [15] examined HNF behavior under nonlinear convection and radiation effects over a stretchable surface, offering new insights into heat augmentation using multiple nanoparticles. Nayak et al. [16] presented a sum-

mary of computations for entropy optimization of nonlinear HNF flows, addressing both assisting and opposing thermal gradients under radiative conditions. Khalatbari et al. [17] explored HNFs and their contributions to thermal and flow performance improvements across diverse engineering platforms. Mishra et al. [18] presented results for unsteady radiative transport in HNF flow over a rotating disk under slip and porosity effects, offering models suitable for transient thermal environments. Upadhyay et al. [19] detected the HNF thermal reflection with inertial effects via the Legendre wavelet collocation technique. Alqarni et al. [20] employed an artificial intelligence simulation to analyze the HNF features for nonparallel surface flow. A study by Abas et al. [21] involves the Joule heating impact to determine the transmission of heat through hybrid nanofluid confined by a disk flow following the rotatory motion. Kumar et al. [22] proposed a machine learning initiative to visualize the hybrid nanofluid applications for thin film flow. An investigation into the interference of slip effects in hybrid nanofluid flow driven by porous medium has been revealed by Abu Bakar et al. [23]. Yasir and Qi [24] inspected the thermal simulations based on the implementation of Yamada-Ota and Xue models.

1.2. Proposed Thermal Problem

The current investigation presents the thermal and solutal perspective of viscoelastic hybrid nanofluid confined by an elastic surface with applications of radiated effects and modified Fourier's approach. The hybrid nanofluid includes the suspension of ferro-oxide (Fe_3O_4) and copper (Cu) nanoparticles along with ethylene glycol ($C_2H_6O_2$) base liquid [25]. The viscoelastic properties arise from the concentrated hybrid nanofluid system and not from pure ethylene glycol. While available research literature focuses on the traditional Fourier heat conduction model and viscous fluid assumptions, this continuation departs by accounting for the advanced Fourier's model, providing the thermal relaxation features and providing a realistic framework for analyzing the finite-speed propagation in assumed decompositions. Furthermore, this analysis accounts for the radiated effects and magnetic force and viscoelastic behavior, an aspect that remains unexplored in the context of hybrid nanofluid. The utilization of the concentration equation further endorsed the understanding of solutal distribution in response to thermal performance. The numerical simulations with implementation of Runge–Kutta integration have been performed to ensure solution convergence.

1.3. Novelty and Applications of the Current Model

The novelty of the performed investigation lies in the integration of multiple advanced physical phenomena- viscoelasticity, radiated effects and HNF interaction within a unified framework. In contrast to already presented models that investigate each of these perspectives in isolation, this contribution provides a realistic platform to analyze the HNF behavior under complex thermal modeling. The proposed results effectively contribute to advanced thermal design of engineering systems where rapid heat removal, controlled temperature regulation and efficient solute transport are necessitated.

2. Problem Formulation

2.1. Flow Assumptions and Governing Equations

A laminar two-dimensional flow of hybrid nanofluid driven by an elastic surface has been focused. The velocity of the moving elastic sheet is defined by $u = u_w = \varpi x$ with a stretching constant ϖ. A representation of the problem is presented in Figure 1. The flow domain lies in the Cartesian plane where the x-component is taken in the direction of the stretched surface while y-axis is attributed along the normal direction [26]. The HNF fluid is assumed to be a decomposition of Fe_3O_4 and Cu nanoparticles suspended in

ethylene glycol ($C_6H_{12}O_6$) as a base fluid, forming a binary HNF mixture. To reflect realistic transport behavior, advanced Fourier's modeling is followed in the energy equation. In addition, thermal radiation is considered via the Rosseland approximation to evaluate its influence on energy transport within the boundary layer. The fluid motion is further subjected to a transverse magnetic field, modeling magnetohydrodynamics (MHD) effects without inducing an electric field or Hall current components. Symbolizing the horizontal velocity component with u, v is the normal component; the HNF temperature is expressed by T, T_∞ endorsed the ambient temperature, C represents the concentration, C_∞ explains the ambient concentration, and the convective temperature is defined by T_f. For such flow constraints, the governing equations are [27,28]:

$$\frac{\partial u}{\partial x} + \frac{\partial v}{\partial y} = 0, \tag{1}$$

$$\begin{aligned} v\frac{\partial u}{\partial y} + u\frac{\partial u}{\partial x} + \frac{k_1}{\rho_{hnf}}\left[u\frac{\partial^3 u}{\partial x \partial y^2} + \frac{\partial^2 u}{\partial y^2}\frac{\partial u}{\partial x} - \frac{\partial^2 u}{\partial x \partial y}\frac{\partial u}{\partial y} + v\frac{\partial^3 u}{\partial y^3}\right] \\ = \frac{\mu_{hnf}}{\rho_{hnf}}\frac{\partial^2 u}{\partial y^2} - \frac{\sigma_{hnf}B_0^2}{\rho_{hnf}}u, \end{aligned} \tag{2}$$

$$\begin{aligned} u\frac{\partial T}{\partial x} + v\frac{\partial T}{\partial y} + \vartheta_1\left[\begin{array}{l} v^2\frac{\partial^2 T}{\partial y^2} + u\frac{\partial u}{\partial x}\frac{\partial T}{\partial x} + u\frac{\partial v}{\partial x}\frac{\partial T}{\partial y} \\ +v\frac{\partial u}{\partial y}\frac{\partial T}{\partial x} + v\frac{\partial v}{\partial y}\frac{\partial T}{\partial y} + u^2\frac{\partial^2 T}{\partial x^2} \\ +2vu\frac{\partial^2 T}{\partial x \partial y} \end{array}\right] \\ = \left(\frac{k_{hnf}}{(\rho C_p)_{hnf}} + \frac{16T_\infty{}^3\sigma^*}{3(\rho C_p)_{hnf}k^*}\right)\frac{\partial^2 T}{\partial y^2}, \end{aligned} \tag{3}$$

$$u\frac{\partial C}{\partial x} + v\frac{\partial C}{\partial y} + \vartheta_2\left[\begin{array}{l} u^2\frac{\partial^2 C}{\partial x^2} + u\frac{\partial C}{\partial x}\frac{\partial u}{\partial x} + u\frac{\partial v}{\partial x}\frac{\partial C}{\partial y} + v\frac{\partial C}{\partial x}\frac{\partial u}{\partial y} \\ +2vu\frac{\partial^2 C}{\partial x \partial y} + v^2\frac{\partial^2 C}{\partial y^2} + v\frac{\partial C}{\partial y}\frac{\partial v}{\partial y} \end{array}\right] = D_B\frac{\partial^2 C}{\partial y^2}. \tag{4}$$

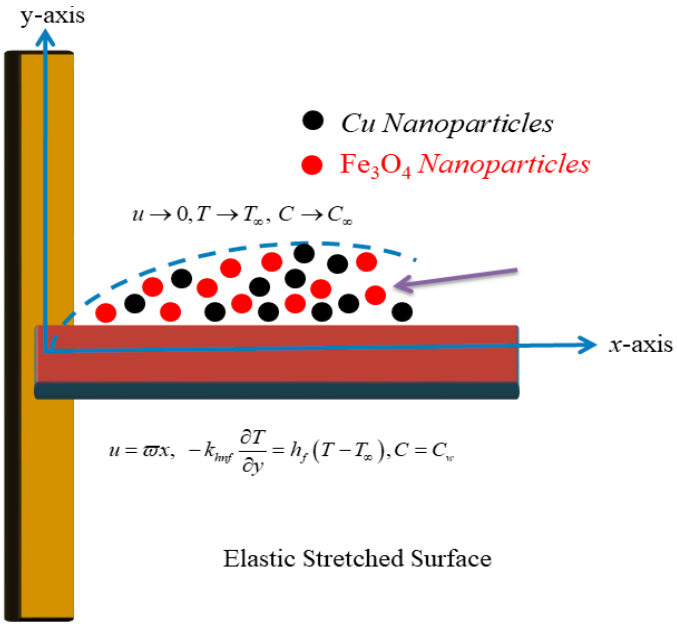


Figure 1. Physical configuration and coordinate system of the proposed model.

The flow undergoes the following flow constraints [28]:

$$\left.\begin{array}{l} u = \varpi x,\ v = 0, -k_{hnf}\frac{\partial T}{\partial y} = h_f(T - T_\infty), C = C_w, y = 0. \\ u \to 0, \frac{\partial u}{\partial y} \to 0, T \to T_\infty, C \to C_\infty, y \to \infty. \end{array}\right\} \tag{5}$$

with ϑ_2 (concentration relaxation coefficient), k_1 (viscoelastic coefficient), ρ_{hnf} (density), μ_{hnf} (dynamic viscosity), σ_{hnf} (electrical conductivity), B_0 (magnetic intensity), ϑ_1 (thermal relaxation time), D_B (Brownian diffusion), k_{hnf} (thermal conductivity), h_f (coefficient of heat transfer), $\left(\rho C_p\right)_{hnf}$ (specific heat capacity), σ_{hnf} (Stefan–Boltzmann constant).

It is remarked that the imposed boundary conditions correspond to a stretching surface framework. Such flow configurations are highly relevant in numerous industrial and engineering applications, including material fabrication, extrusion technologies, thermal regulation systems, and polymer processing environments.

The flow problem is now simplified by considering the following flow variables [28]:

$$\theta(\xi) = \frac{T - T_\infty}{T_f - T_\infty},\ v = -\sqrt{\nu_f \varpi} f(\xi), u = \varpi x f'(\xi), S(\xi) = \frac{C - C_\infty}{C_w - C_\infty},\ \xi = \sqrt{\frac{\varpi}{\nu_f}} y. \quad (6)$$

The formulated system is:

$$A_2 f''' + A_1\left(ff'' - f'^2\right) - \alpha\left(2f'f''' - f''^2 - ff''''\right) - A_1 H f' = 0, \quad (7)$$

$$(A_5 + R)\theta'' + Pr\left[-A_4 f\theta' - A_4\lambda_1\left(ff'\theta' + f^2\theta''\right)\right] = 0, \quad (8)$$

$$S'' + \gamma f S' - \lambda_2\gamma\left(ff'S' + f^2 S''\right) = 0. \quad (9)$$

with:

$$\begin{aligned} &f(0) = 0, f'(0) = 1, A_5\theta'(0) = -Bi[1 - \theta(0)], S(0) = 1, \\ &f'(\infty) \to 0, f''(\infty) \to 0, \theta(\infty) \to 0, S(\infty) \to 0. \end{aligned} \quad (10)$$

with Bi (Biot number), R (radiation parameter), α (viscoelastic parameter), $\gamma = \nu_f / D_B$ (Schmidt number), λ_2 (concentration relaxation constant), Pr (Prandtl number), λ_1 (thermal relaxation constant) and H (Hartmann number) which are expressed as:

$$\begin{aligned} \alpha = \frac{k_1\varpi}{\rho_f\nu_f}, \gamma = \frac{\nu_f}{D_B},\ H = \frac{\sigma_{hnf}{B_0}^2}{\rho_f\varpi},\ R = \frac{16{T_\infty}^3\sigma^*}{3k_{hnf}k^*},\ \lambda_1 = \vartheta_1\varpi, \\ \lambda_2 = \vartheta_2\varpi,\ Pr = \nu_f\left(\frac{\rho C_{p_f}}{k_f}\right),\ Bi = \left(h_f/k_{hnf}\right)\sqrt{\nu_f\varpi} \end{aligned}$$

The physical quantities are further defined by:

$$A_1 = \frac{\rho_{hnf}}{\rho_f}, A_2 = \frac{\mu_{hnf}}{\rho_f}, A_3 = \frac{\sigma_{hnf}}{\sigma_f}, A_4 = \frac{\left(\rho C_p\right)_{hnf}}{\left(\rho C_p\right)_f}, A_5 = \frac{k_{hnf}}{k_f} \quad (11)$$

The HNF consists of ethylene glycol base liquid decomposed with Fe_3O_4 and Cu nanoparticles.

The suspension of Fe_3O_4 and Cu nanoparticles is endorsed due to peak thermal management and uniform magnetic relevance, which presents the synergistic features that impel the transfer of heat effectively. The role of ethylene glycol as a base material is justified due to stable thermo-physical properties, chemical reliability and wide applications in thermal management systems, making the HNF more suitable for advanced energy and cooling systems. Table 1 presents the numerical range of base fluid and nanoparticles. Table 2 illustrates the expressions used to determine the HNF dynamics.

Table 1. Thermo-physical features of HNF [29].

Physical Properties	Cu	Fe_3O_4	$C_2H_6O_2$
ρ (kgm^{-3})	8933	5180	1114
C_p (Jkg.k)	385	670	2415
κ (W.(m.k))	401	9.7	0.252

Table 2. Mathematical relevance of nanofluids and hybrid nanomaterials [25,28].

Physical Characteristics	Mathematical Expressions
Density	$\rho_{nf} = (1-\varphi)\rho_f + \varphi\rho_s$ $\rho_{hnf} = (1-\varphi_2)\left[(1-\varphi_1)\rho_f + \varphi_1\rho_{s1}\right] + \varphi_2\rho_{s2}$
Heat Capacity	$(\rho C_p)_{nf} = \left[(1-\varphi)(\rho C_p)_f + \varphi(\rho C_p)_s\right]$ $(\rho C_p)_{nf} = (1-\varphi_2)\left[(1-\varphi_1)(\rho C_p)_f + \varphi_1(\rho C_p)_{s1}\right] + \varphi_2(\rho C_p)_{s2}$
Dynamic Viscosity	$\mu_{nf} = \frac{\mu_f}{(1-\varphi)^{2.5}}$ $\mu_{nf} = \frac{\mu_f}{(1-\varphi_1)^{2.5}(1-\varphi_2)^{2.5}}$
Thermal Conductivity	$k_{nf} = \frac{k_s+(n-1)k_f-(n-1)\phi(k_f-k_s)}{k_s+(n-1)k_f+(n-1)\phi(k_f-k_s)} * k_f$ $k_{hnf} = \frac{k_{s1}+(n-1)k_f-(n-1)\varphi_1(k_f-k_{s1})}{k_{s1}+(n-1)k_f+\varphi_1(k_f-k_{s1})} * k_f$ $k_{hnf} = \frac{k_{s2}+(n-1)k_{bf}-(n-1)\varphi_2(k_{bf}-k_{s2})}{k_{s2}+(n-1)k_{bf}+\varphi_2(k_{bf}-k_{s2})} * k_f$

2.2. Engineering Quantities

The skin friction coefficient, local Sherwood number, and local Nusselt number are [28]:

$$\begin{aligned} C_f &= \frac{\tau_w}{\rho u_w^2}, \tau_w = \mu_{hnf}\left[\left(\frac{\partial u}{\partial y}\right) + k_0\left(u\frac{\partial^2 u}{\partial x \partial y} + v\frac{\partial^2 u}{\partial y^2} - 2\frac{\partial u}{\partial y}\frac{\partial v}{\partial y}\right)\right]_{y=0}, \\ Nu &= \frac{xq_w}{k(T_f - T_\infty)}, q_w = -\left(k_{hnf} + \frac{16T_\infty^3\sigma^*}{3k^*}\right)\left(\frac{\partial T}{\partial y}\right)_{y=0}, \\ Sh_x &= \frac{xJ_w}{D_B(C_w - C_\infty)}, \; J_w = -D_B\left(\frac{\partial C}{\partial y}\right)_{y=0}. \end{aligned} \tag{12}$$

$$\begin{aligned} Re_x^{1/2} C_f A_1 &= A_2[f'' + K(3f'f'' - ff''')]_{\xi=0}, \\ Re_x^{-1/2} Nu_x &= -(1 + A_5 Nr)\theta'(0), \\ Sh_x(Re_x)^{-1/2} &= -S'(0). \end{aligned} \tag{13}$$

3. Solution Methodology

The present model is numerically explored using the shooting method, a robust computational approach commonly employed in the analysis of transport phenomena and nonlinear fluid flow systems. This technique proves especially effective when analytical solutions are infeasible due to the presence of strong nonlinearities and coupled differential equations. The core idea of the shooting strategy lies in recasting the higher order approximations to system of first order. This reformulation enables iterative refinement, where initially guessed values are adjusted to satisfy terminal boundary constraints. Introducing following transformations:

$$\begin{aligned} &f = \kappa_1, f' = \kappa_2, f'' = \kappa_3, f''' = \kappa_4, f^{iv} = \kappa_4' \\ &\theta = \kappa_5, \theta' = \kappa_6, \theta'' = \kappa_6', \\ &S = \kappa_7, S' = \kappa_8, S'' = \kappa_8'. \end{aligned} \quad , \tag{14}$$

$$\kappa_4' = \frac{-1}{\alpha\kappa_1}\left[A_2\kappa_4 - A_1\left(\kappa_2^2 - \kappa_1\kappa_3\right) - A_3 H\kappa_2 - \alpha\left(2\kappa_2\kappa_4 - \kappa_3^2\right)\right], \tag{15}$$

$$\kappa_6{}' = \frac{-Pr}{((A_5 + Nr) - PrA_4\lambda_1{\kappa_1}^2)[-A_4\kappa_6 - A_4\lambda_1\kappa_1\kappa_2\kappa_6]}, \tag{16}$$

$$\kappa_8{}' = \frac{-\gamma\kappa_1\kappa_8 + \lambda_2(\kappa_1\kappa_2\kappa_8)}{(1 - \lambda_2{\kappa_1}^2)} \tag{17}$$

with:

$$\begin{aligned} &\kappa_1(0) = 0, \kappa_2(0) = 1, A_5\kappa_6(0) = -Bi[1 - \kappa_5(0)], \kappa_5(0) = 1, \\ &\kappa_2(\infty) \to 0, \kappa_3(\infty) \to 0, \kappa_5(\infty) \to 0, \kappa_7(\infty) \to 0. \end{aligned} \tag{18}$$

The iterative simulations are repeated until the accuracy of 10^{-6} is achieved. The computations are performed by maintaining the size of $\Delta\eta = 0.002$. MATLAB 2017 computational tool has been used to perform the simulations. The CPU time ranges from 10 to 90 s depending upon different modeled parameters and grid resolution.

4. Validation of Results

In order to validate the accuracy of the computed solution, a comparative analysis is worked out in Table 3 with the already claimed investigation of Turkyilmazoglu [30] and Hayat et al. [31]. A favorable solution accuracy is determined with both studies, which confirms the accuracy of numerically predicted data.

Table 3. Results for $f''(0)$ with the investigation of Turkyilmazoglu [30] and Hayat et al. [31] when $A_1 = A_2 = 1$ and $K = 0$.

H	Turkyilmazoglu [30]	Hayat et al. [31]	Current Results
0.5	−1.2247448	−1.224747	−1.2247451
1.5	−1.5811388	−1.581147	−1.581142
2.0	−1.7320508	−1.732057	−1.732056

5. Physical Interpretation of Results

The heat transfer has been studied to predict the HNF dynamics containing the Cu and Fe_3O_4 nanoparticles with ethylene glycol ($C_2H_6O_2$) base fluid. The shooting method is employed to simulate the computations. This section accounts for the discussion on the thermal perspective of hybrid nanofluid for both mono nanofluid $Cu/C_2H_6O_2$ and hybrid nanofluid $(Cu–Fe_3O_4)/C_2H_6O_2$. Figure 2a determines the influence of Hartmann number H on velocity profile $f'(\xi)$. A stronger magnetic force leads to a reduction in $f'(\xi)$, which is physically associated with the implementation of the Lorentz force. Such magnetic damping appeared for both HNF and MNF; however, MNF experienced a pronounced velocity reduction. Thus, it can be stated that the HNF maintains higher velocity under the same magnetic field. Figure 2b shows a similar trend when the viscoelastic parameter is varied: increasing α (from 0.2 to 1.0) causes a pronounced decrease in $f'(\xi)$ for both nanofluids. Greater fluid elasticity leads to more significant internal stress that opposes the flow, thus lower uniform velocity profiles occur as α rises. In this case, however, the hybrid nanofluid's velocity is more strongly attenuated by viscoelastic effects than the mono-nanofluid's. The HNF exhibits a larger drop in $f'(\xi)$ with the increase in α, but the mono-nanofluid retains slightly higher velocities under the same elastic conditions. This indicates that the presence of both Cu and Fe_3O_4 nanoparticles amplifies the elasticity-induced flow resistance in the hybrid nanofluid, while the mono-nanoparticle fluid is less affected by the increase in α.

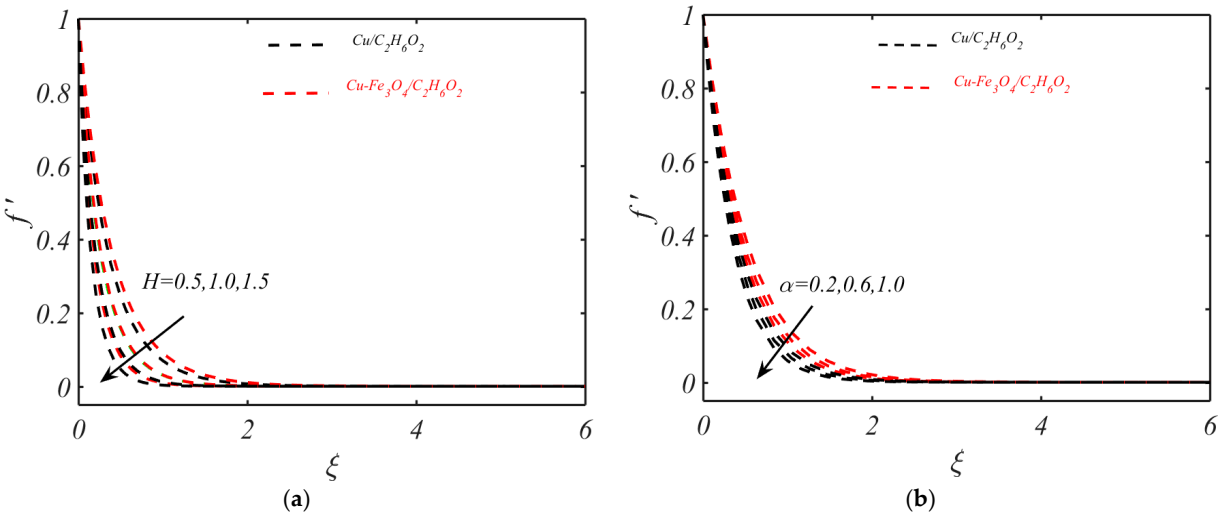


Figure 2. Analysis of velocity profile f' for (**a**) H (**b**) α.

To study the behavior of temperature distribution θ due to the viscoelastic parameter α, Figure 3a is proposed. An increase in α enhances the thermal transport, with the hybrid formulation exhibiting a more significant rise in heat transfer efficiency. Figure 3b explores the behavior of θ under the influence of the Biot number Bi, showing that greater Bi values lead to improved thermal profiles for both types of nanofluids. This is attributed to the direct relationship between Bi and the convective heat transfer coefficient, highlighting the role of convective boundary conditions in enhancing internal thermal conduction, especially in HNFs. Figure 3c illustrates the effect of the increase in the nanoparticle volume fraction (ϕ_1, ϕ_2) on the temperature profile. It is observed that the hybrid suspension $(Cu–Fe_3O_4)/C_2H_6O_2$ shows superior thermal enhancement while a single nanoparticle accomplishes less. Figure 3d demonstrates that increasing the radiated number R leads to an elevated temperature profile. This radiative enhancement is more pronounced in HNFs, reflecting their potential to increase thermal energy distribution and heat exchange in advanced energy systems. Lastly, Figure 3e illustrates the effects of the thermal relaxation time λ_T on θ. As λ_T increases, a noticeable reduction in the temperature profile is observed, particularly for the mono-nanofluid, suggesting a delayed thermal response due to non-Fourier heat conduction effects.

The results for the investigation of concentration distribution S due to Schmidt number γ have been prepared in Figure 4a. It is observed that as γ increases, the concentration profile decreases. The reduction in concentration distribution S is physically attributed to the reduction in mass diffusivity, which opposes the dispersion of the species. In Figure 4b, the effect of the concentration relaxation parameter λ_2 is analyzed; it reveals that higher values of λ_2 cause a noticeable reduction in concentration. Physically, a higher concentration relaxation number means that the nanoparticle concentration field requires a long time to respond to the local concentration gradients. Such a delayed diffusion process weakens the nanoparticle transport from higher to lower concentration regions, resulting in a thinner concentration boundary layer and consequently a lower concentration level.

Figure 4c presents the variation of S with the viscoelastic parameter α; it is observed that the increase in α leads to higher concentrations. Physically, the viscoelastic parameter contributes to the elastic nature of the fluid and its capability to store deformation energy. When the fluid exhibits larger resistance to rapid deformation, the effects of the viscoelastic parameter become more prominent. For hybrid nanofluid $Cu–Fe_3O_4/C_2H_6O$, this improvement in concentration profile becomes more pronounced due to synergistic interaction

between two different types of nanoparticles, which alters the rheological dynamics of this suspension and strengthens the viscoelastic response.

Figure 5a explores the variation in the skin friction coefficient with the Hartmann number H at different values of the viscoelastic parameter α. The skin friction is very important in fluid dynamics; in fact, it represents the shear stress exerted near the surface due to viscosity and is crucial for the optimization of flow-system efficiency. As α increases, the wall shear stress is found to intensify, highlighting its significance in aerodynamic applications where minimizing drag is essential for improving vehicle and aircraft performance. Meanwhile, Figure 5b presents the results for Sherwood number versus Schmidt number γ for increasing H. The behavior shows a consistent decrement in mass transfer rate against H, demonstrating its suppressive influence on concentration boundary layers.

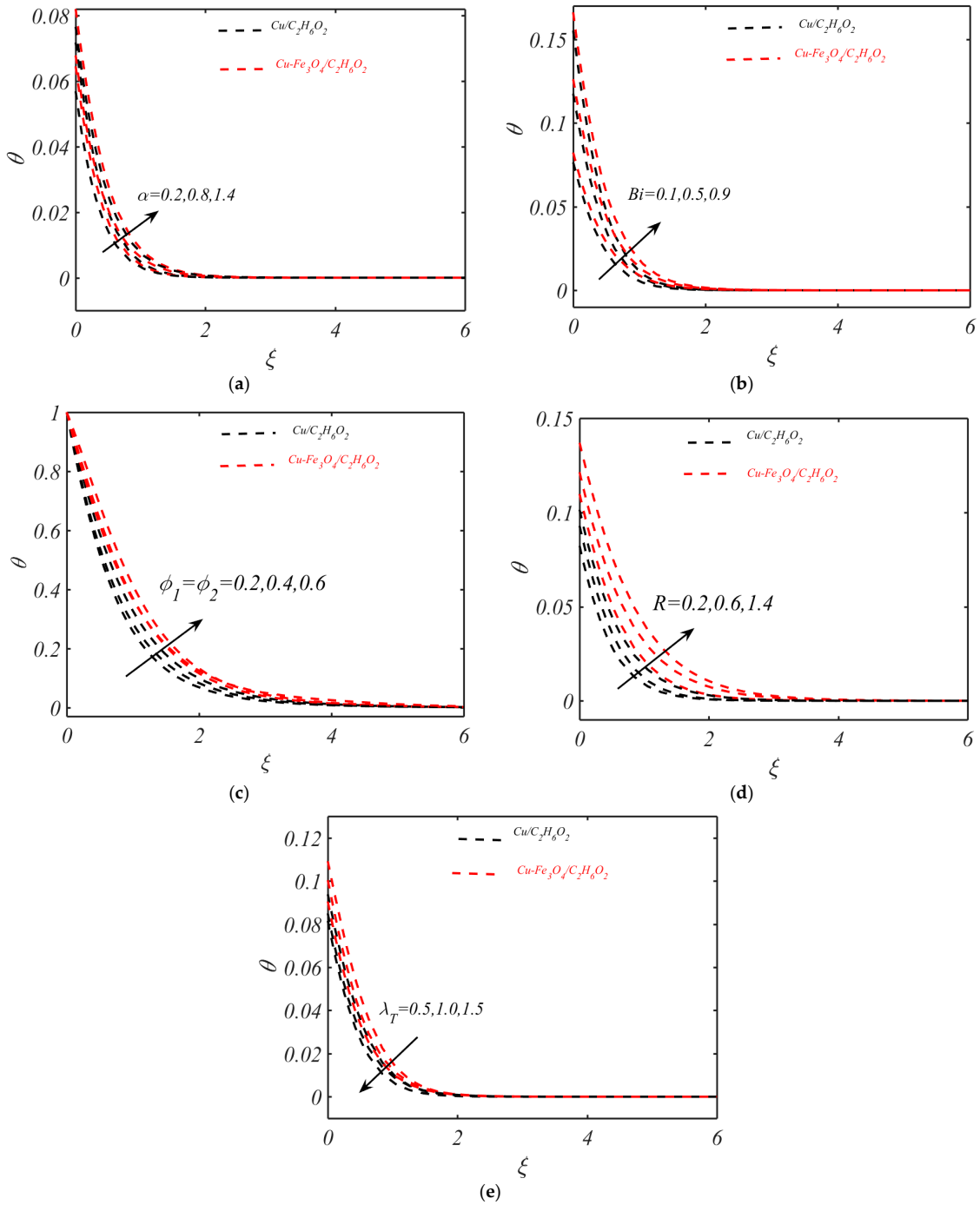


Figure 3. Effect of (**a**) α; (**b**) Bi; (**c**) ϕ_1, ϕ_2; (**d**) R; (**e**) λ_1 on the temperature field θ.

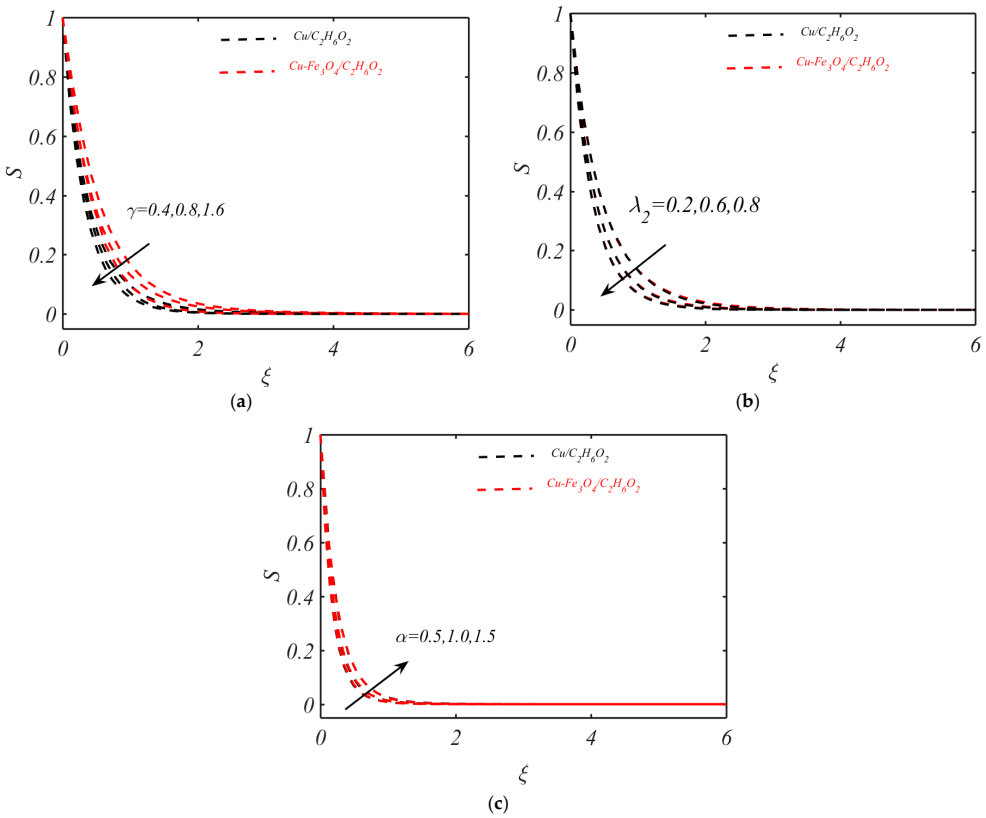


Figure 4. Effect of (**a**) γ; (**b**) λ_2; (**c**) α on the concentration profile.

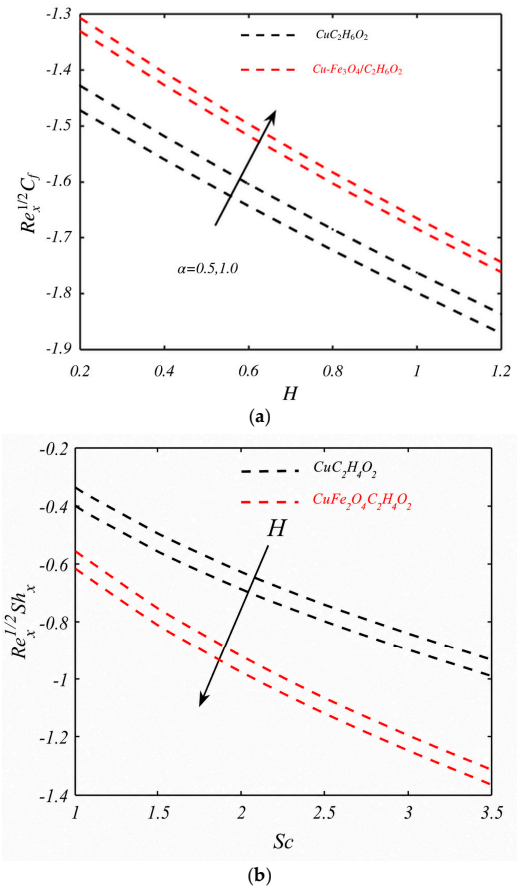


Figure 5. (**a**) Effects of H and α on the skin friction coefficient and (**b**) effects of H and Sc on the Sherwood number.

https://doi.org/10.3390/mca31040129

6. Conclusions

- The velocity profile diminishes with increasing Hartmann number and viscoelastic parameter, due to enhanced Lorentz and elastic resistance, with HNFs offering better flow control compared to mono-nanofluids.
- More impressive thermal results are examined for HNF $(Cu–Fe_3O_4)/C_2H_6O_2$ as compared to Cu-based MNF.
- An intensified thermal profile is examined for the radiated parameter, providing applications to high-energy systems and optimized heat transfer phenomena.
- Larger concentration relaxation number and Schmidt parameter suppress the concentration profile, justifying the role of non- instantaneous chemical species and controlled mass diffusivity.
- The presence of a chemical reaction parameter reduces mass concentration, where HNF suspension claims better resilience under the reactive flow conditions.
- Boosted wall shear force is examined when viscoelastic effects are prominent, which is important to regulate the surface drag and momentum transfer.
- The Sherwood number and Nusselt number are suppressed due to stronger magnetic force, indicating a damping impact on both thermal and concentration gradients.
- For all observations, the HNF accomplishes peak thermal relevance and flow behavior as compared to MNF, affirming its capability in modern engineering applications.

6.1. Applications of the Current Model

The outcomes of the proposed modeling incorporate the potential of viscoelastic hybrid nanofluid in a variety of advanced fluid and thermal systems. The analyzed enhancement in heat transfer and flow control by using the $Cu–Fe_3O_4$/ethylene glycol-based HNF makes this suspension a strong candidate for applications in thermal heat exchangers, high-performance HVAC systems and microelectronics cooling. The capability to manipulate the wall shear force and thermal profiles through viscoelastic hybrid nanofluid modeling justifies its relevance in aerospace engineering and automotive systems, especially in drag control and thermal shielding. Moreover, the understanding of concentration and radiation impact on complex flow regimes makes this model versatile and applicable for thermal solar collectors, geothermal management systems and biomedical applications. Overall, the HNF model incorporates a versatile and efficient approach to improving the heat and mass transfer phenomenon in advanced energy and engineering systems.

6.2. Future Recommendations

Future studies can extend this framework by incorporating transient flows, complex geometries, entropy generation, slip effects, thermophoretic features, and Hall effects. Moreover, experimental validation and the inclusion of machine learning-based optimization could enhance predictive modeling and practical implementation in real-world energy, biomedical, and aerospace systems.

Funding: This project was funded by the Deanship of Scientific Research (DSR) at King Abdulaziz University, Jeddah, Saudi Arabia, under grant no. (IPIP-1171-135-2025). The author, therefore, acknowledges DSR with thanks for technical and financial support.

Data Availability Statement: Data are provided within the manuscript.

Conflicts of Interest: The author declares that he has no known competing financial interests or personal relationships that could have appeared to influence the work reported in this paper.

Nomenclature

(x, y)	Coordinate axis (ms^{-1})
(u, v)	Velocity components (m)
ϖ	Stretched constant (s^{-1})
C	Concentration $\left(\mathrm{kgm}^{-3}\right)$
T_∞	Ambient temperature (K)
T	Temperature (K)
C_w	Surface concentration $\left(\mathrm{kgm}^{-3}\right)$
C_∞	Ambient concentration $\left(\mathrm{kgm}^{-3}\right)$
μ_{hnf}	Dynamic viscosity $\left(\mathrm{kgm}^{-1}\mathrm{s}^{-1}\right)$
σ_{hnf}	Electrical conductivity $\left(\mathrm{Sm}^{-1}\right)$
B_0	Magnetic intensity $\left(\mathrm{kgs}^{-2}\mathrm{A}^{-1}\right)$
k_{hnf}	Thermal conductivity $(\mathrm{m}^2\mathrm{s}^{-1})$
h_f	Coefficient of heat transfer
$\left(\rho C_p\right)_{hnf}$	Specific heat capacity $\left(\mathrm{m}^2\mathrm{s}^{-2}\mathrm{K}^{-1}\right)$
σ_{hnf}	Stefan–Boltzmann constant $\left(\mathrm{Wm}^{-2}\mathrm{K}^{-4}\right)$
ρ_{hnf}	Density $\left(\mathrm{kgm}^{-3}\right)$
D_B	Brownian diffusion $(\mathrm{m}^2\mathrm{s}^{-1})$
ϑ_2	Concentration relaxation coefficient
k_1	Viscoelastic coefficient
ϑ_1	Thermal relaxation time
D_B	Brownian diffusion
Bi	Biot number
R	Radiation parameter
α	Viscoelastic parameter
γ	Schmidt number
λ_2	Concentration relaxation constant
Pr	Prandtl number
λ_1	Thermal relaxation constant
H	Hartmann number

References

1. Hassan, M.; Marin, M.; Alsharif, A.; Ellahi, R. Convective heat transfer flow of nanofluid in a porous medium over wavy surface. *Phys. Lett. A* **2018**, *382*, 2749–2753. [CrossRef]
2. Nadeem, S.; Akhtar, S.; Abbas, N. Heat transfer of Maxwell base fluid flow of nanomaterial with MHD over a vertical moving surface. *Alex. Eng. J.* **2020**, *59*, 1847–1856. [CrossRef]
3. Mebarek-Oudina, F.; Chabani, I. Review on nano-fluids applications and heat transfer enhancement techniques in different enclosures. *J. Nanofluids* **2022**, *11*, 155–168. [CrossRef]
4. Bhatti, M.; Abbas, M.A.; Muhammad, S. Optimizing fluid flow efficiency: Third-grade HNF flow with electro-magneto-hydrodynamics in confined vertical spaces. In *Nanofluids*; Elsevier: Amsterdam, The Netherlands, 2024; pp. 243–275.
5. Siddiqui, A.A.; Turkyilmazoglu, M. Film flow of nano-micropolar fluid with dissipation effect. *CMES-Comput. Model. Eng. Sci.* **2024**, *140*, 2487–2512. [CrossRef]
6. Khan, U.; Rafique, K.; Mahmood, Z. Significance of unsteady rotating flow of nanofluid with nanoparticles aggregation and impacts of slip conditions and variable viscosity. *Numer. Heat Transf. Part A Appl.* **2025**, *86*, 3233–3260.
7. Gupta, R.; Wakif, A. Computing neural network to analyze heat and mass transfer in the flow of nanofluid between two disks. *Numer. Heat Transf. Part A Appl.* **2025**, *86*, 2539–2568.
8. Puneeth, V.; Sini, K.; Clair, T.; Anwar, M.S. Flow of nanofluid past a stretching cylinder subject to Thompson and Troian slip in the presence of gyrotactic microorganisms. *Multiscale Multidiscip. Model. Exp. Des.* **2025**, *8*, 84.
9. Galal, A.M.; Mishra, S.; Baithalu, R.; Kallel, M.; Panda, S.; Chamkha, A.J.; Ali, R.; Afshar, S. Three-dimensional flow of nanofluid through a vertical channel considering KKL model: Hydrothermal analysis via response surface methodology. *J. Taiwan Inst. Chem. Eng.* **2025**, *168*, 105931. [CrossRef]

10. Hamid, A.; Maqsood, Z.; Farooq, N. Significance of activation energy and binary chemical reaction effects on mixed convection Falkner–Skan flow of nanofluid along a wedge. *Int. J. Thermofluids* **2025**, *26*, 101070. [CrossRef]
11. Gangadhar, K.; Chandrika, G.N.; Dinarvand, S. Investigation into silver-engine oil nanoliquid convinced by Riga surface: Deviations in three binary nanofluids. *Mod. Phys. Lett. B* **2025**, *39*, 2450385. [CrossRef]
12. Reddy, M.V.; Nath, J.M.; Ali, F.; Das, T.K.; Khan, U.; Garayev, M. Implementation of homotopy analysis method for entropy-optimized two-phase nanofluid flow in a bioconvective non-Newtonian model with thermal radiation. *J. Radiat. Res. Appl. Sci.* **2025**, *18*, 101218. [CrossRef]
13. Ramesh, D.; Babu, M.M.; Prakash, G.B.; Rani, K.J.; Praveen, J.P.; Reddy, G.V.R. Magneto-Hydrodynamic Effects on Heat and Mass Transfer in HNF Flow over A Stretched Sheet with Cattaneo-Christov Model. *CFD Lett.* **2024**, *16*, 105–117.
14. Manzoor, U.; Imran, M.; Muhammad, T.; Waqas, H.; Alghamdi, M. Heat transfer improvement in HNF flow over a moving sheet with magnetic dipole. *Waves Random Complex Media* **2024**, *34*, 4494–4508.
15. Nasir, S.; Sirisubtawee, S.; Gul, T.; Juntharee, P.; Alghamdi, W.; Ali, I. Thermal characteristics of nonlinear convection and radiation for the flow of tri-HNFs over stretchable surface with energy source. *Surf. Rev. Lett.* **2022**, *29*, 2250153. [CrossRef]
16. Nayak, M.K.; Mabood, F.; Dogonchi, A.S.; Ramadan, K.M.; Tlili, I.; Khan, W.A. Entropy optimized assisting and opposing non-linear radiative flow of HNF. *Waves Random Complex Media* **2025**, *35*, 1389–1410. [CrossRef]
17. Khalatbari, S.; Jalili, P.; Jalili, B.; Ganji, D.D. Investigating the improvement of heat transfer and flow characteristics of HNFs: A comprehensive review. *Proc. Inst. Mech. Eng. Part E J. Process Mech. Eng.* **2025**, 09544089251318785. [CrossRef]
18. Mishra, S.; Haq, I.; Baithalu, R.; Panda, S.; Saeed, A. Transient radiative flow of HNF under slip effects over an impermeable spinning disk with porous material. *Partial. Differ. Equ. Appl. Math.* **2025**, *14*, 101154. [CrossRef]
19. Upadhyay, S.; Upreti, H.; Pandey, A.K. Three-dimensional flow of HNF through Darcy-Forchheimer porous surface: A Legendre wavelet collocation approach. *Numer. Heat Transf. Part A Appl.* **2025**, *86*, 2155–2179.
20. Alqarni, M.; Alghamdi, S.; Ullah, M.Z.; Aljohani, M.; Gul, T.; Mahmoud, E.E. The flow of HNFs between nonparallel stretching walls using neural network and control volume finite element method. *Int. J. Numer. Methods Heat Fluid Flow* **2025**, *35*, 2484–2508. [CrossRef]
21. Abas, S.A.; Ullah, H.; Fiza, M.; Jan, A.U.; Akgül, A.; Hendy, A.; Elaissi, S.; Mahariq, I.; Khan, I. Effects of Joule heating on MHD flow of HNF between rotating disks. *J. Radiat. Res. Appl. Sci.* **2025**, *18*, 101341. [CrossRef]
22. Kumar, M.D.; Dharmaiah, G.; Yook, S.-J.; Raju, C.; Shah, N.A. Deep learning approach for predicting heat transfer in water-based HNF thin film flow and optimization via response surface methodology. *Case Stud. Therm. Eng.* **2025**, *68*, 105930. [CrossRef]
23. Yasir, M.; Qi, H. Heat transfer insight of ternary hybrid nanofluid over an oscillatory heated surface with Yamada-Ota and Xue models in fixed and moving frames. *Int. Commun. Heat Mass Transf.* **2026**, *172*, 110452. [CrossRef]
24. Abu Bakar, S.; Wahid, N.S.; Arifin, N.M.; Khashi'ie, N.S. The flow of HNF past a permeable shrinking sheet in a Darcy–Forchheimer porous medium with second-order velocity slip. *Waves Random Complex Media* **2025**, *35*, 46–63. [CrossRef]
25. Pastoriza-Gallego, M.J.; Lugo, L.; Legido, J.L.; Piñeiro, M.M. Rheological non-Newtonian behaviour of ethylene glycol-based Fe2O3 nanofluids. *Nanoscale Res. Lett.* **2011**, *6*, 560. [CrossRef] [PubMed]
26. Turkyilmazoglu, M. A unified Stefan–Scott theory for squeeze-film lubrication between non-uniformly deforming boundaries. *Int. Commun. Heat Mass Transf.* **2026**, *174*, 111012. [CrossRef]
27. Aïboud, S.; Saouli, S. Second law analysis of viscoelastic fluid over a stretching sheet subject to a transverse magnetic field with heat and mass transfer. *Entropy* **2010**, *12*, 1867–1884. [CrossRef]
28. Khan, S.U.; Maatki, C.; Ishaq, M.; Alrasheedi, N.H.; Adnan; Kolsi, L. Heat Transfer Assessment Due to Radiated Tri-Hybrid Nanofluid with Dissipative Heating and Cattaneo-Christov Analysis: Biomedical and Advanced Energy Applications. *Z. Angew. Math. Mech.* **2025**, *105*, e70113. [CrossRef]
29. Wang, F.; Fatunmbi, E.; Adeosun, A.; Salawu, S.; Animasaun, I.; Sarris, I. Comparative analysis between copper ethylene-glycol and copper-iron oxide ethylene-glycol nanoparticles both experiencing Coriolis force, velocity and temperature jump. *Case Stud. Therm. Eng.* **2023**, *47*, 103028. [CrossRef]
30. Turkyilmazoglu, M. The analytical solution of mixed convection heat transfer and fluid flow of an MHD viscoelastic fluid over a permeable stretching surface. *Int. J. Mech. Sci.* **2013**, *77*, 263–268. [CrossRef]
31. Hayat, T.; Mustafa, M.; Pop, I. Heat and mass transfer for Soret and Dufour's effect on mixed convection boundary layer flow over a stretching vertical surface in a porous medium filled with a viscoelastic fluid. *Commun. Nonlinear Sci. Numer. Simul.* **2010**, *15*, 1183–1196. [CrossRef]

Disclaimer/Publisher's Note: The statements, opinions and data contained in all publications are solely those of the individual author(s) and contributor(s) and not of MDPI and/or the editor(s). MDPI and/or the editor(s) disclaim responsibility for any injury to people or property resulting from any ideas, methods, instructions or products referred to in the content.